3D-Foam-Structured Nitrogen-Doped Graphene-Ni Catalyst for Highly Efficient Nitrobenzene Reduction

Zhiyong Wang, Yuan Pu, Dan Wang, and Jie Shi
State Key Laboratory of Organic-Inorganic Composites, Beijing University of Chemical Technology, Beijing 100029, China

Research Center of the Ministry of Education for High Gravity Engineering and Technology, Beijing University of Chemical Technology, Beijing 100029, China

Jie-Xin Wang and Jian-Feng Chen
State Key Laboratory of Organic-Inorganic Composites, Beijing University of Chemical Technology, Beijing 100029, China

Research Center of the Ministry of Education for High Gravity Engineering and Technology, Beijing University of Chemical Technology, Beijing 100029, China

Beijing Advanced Innovation Center for Soft Matter Science and Engineering, Beijing University of Chemical Technology, Beijing 100029, China

DOI 10.1002/aic.16016
Published online November 6, 2017 in Wiley Online Library (wileyonlinelibrary.com)

We report the preparation of a porous 3D-foam-structured nitrogen-doped graphene-Ni (NG/NF) catalyst and the evaluation of its performance in the reduction of nitrobenzene (NB) through detailed studies of the kinetics. The NG/NF catalyst showed a significantly higher reaction rate than pure Ni foam (NF). Moreover, the separation of the 3D-foam-structured catalyst from the products was more convenient than that of NG powdered catalysts. The obtained kinetics data fit well to the Langmuir-Hinshelwood model, with an error ratio below 10%. Density functional theory (DFT) calculations indicated that the adsorption of sodium borohydride ($NaBH_4$) on the NG/NF surface was stronger than that of NB, which strongly agreed with the kinetic parameters determined from the Langmuir-Hinshelwood model. The excellent catalytic efficiency of the 3D-foam-structured catalyst combined with the knowledge of the kinetics data make this catalyst promising for application in larger scale nitrobenzene reduction. © 2017 American Institute of Chemical Engineers *AIChE J*, 64: 1330–1338, 2018

Keywords: nitrogen-doped graphene, 3D-foam-structured catalysts, nitrobenzene reduction, Langmuir-Hinshelwood model, density functional theory calculation

Introduction

The reduction of nitrobenzene (NB) to aniline (AB) is an important catalytic reaction because the reaction product is one of the most important intermediates in the production of rubber,[1] coatings,[2] organic pigments,[3] and pesticides.[4,5] In terms of environmental protection, NB is listed as a priority pollutant in drinking water in many countries.[6] The traditional noncatalytic treatment methods that use Fe as a reducing agent generate large amounts of organic wastewater and toxic solid waste.[7–9] Therefore, noble metal-based catalysts, such as those containing Au, Pd, and Pt, have been used for the catalytic reduction of nitrobenzene in the aniline production industry.[10–12] However, the scalability of the industrial applications of these catalysts is limited due the limited reserves and high cost of noble metals. Therefore, the development of environmentally friendly, low-cost, and efficient catalysts for this reduction reaction is critical.

Carbon nanomaterials have received intense scientific interest and have found wide application in the fields of biology, energy, and catalysis, among many others.[13–16] Research on the catalytic use of two-dimensional (2D) graphene has increased significantly over the last 10 years.[17,18] Tremendous progress has been made on 2D layered materials, and many review articles have focused on the synthetic strategies, physical properties, and applications of such materials.[19–22] In particular, nitrogen-doped graphene (NG) has been demonstrated as an efficient metal-free catalyst in many industrially important reactions, such as styrene synthesis, cyclohexane oxidation, benzene hydroxylation, and the oxygen reduction reaction,[23,24] However, the application of powdered 2D graphene catalysts in practical liquid-solid or gas-liquid-solid

Additional Supporting Information may be found in the online version of this article.

Correspondence concerning this article should be addressed to D. Wang at wangdan@mail.buct.edu.cn.

© 2017 American Institute of Chemical Engineers

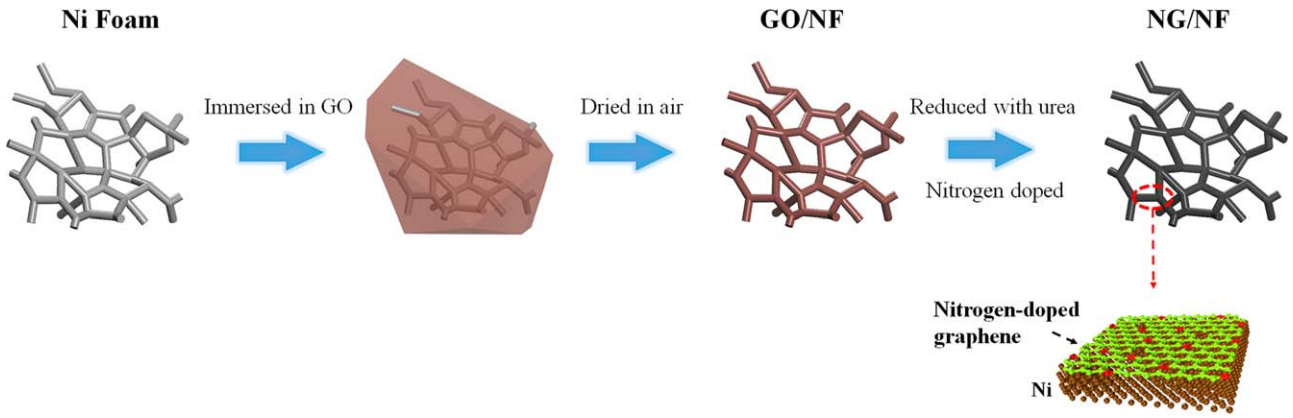

Figure 1. Schematic illustration of the preparation of NG/NF.

[Color figure can be viewed at wileyonlinelibrary.com]

multiphase reaction systems has been met with some problems, such as aggregation and the bleeding of the graphene powders.[25,26] As one technique for improving the properties, structured catalysts have many advantages over conventional pellet or powdered catalysts in terms of the transport characteristics and macro-kinetics of heterogeneous catalytic reactions.[27] Nickel foam (NF), which can be easily fabricated and is an inexpensive commercial material, exhibits outstanding heat transfer properties, a desirable 3D open-pore structure and suitable mechanical strength and has been widely employed as a substrate template in the preparation of 3D-structured graphene.[28,29] For example, the combination of 2D

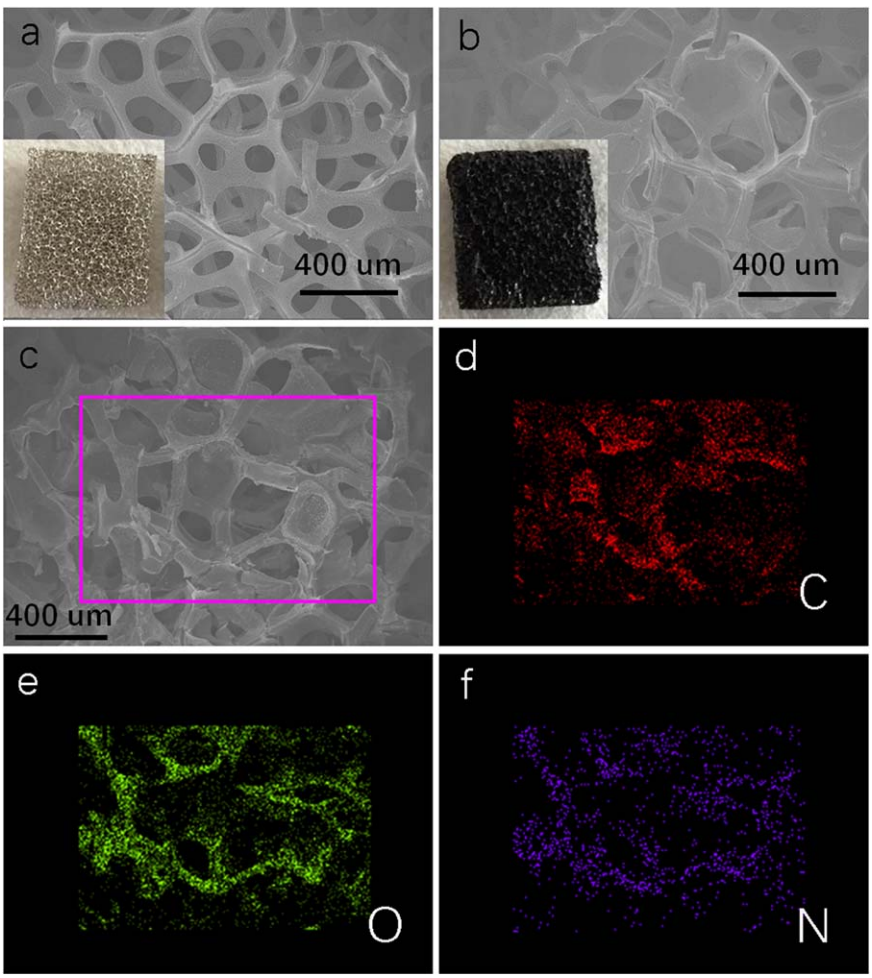

Figure 2. SEM images of (a) NF and (b) NG/NF; the insets are the corresponding digital photographs of 1 cm × 1 cm × 0.15 cm sections. (c) SEM image corresponding to the elemental mapping images of (d) C, (e) O, and (f) N in NG/NF.

[Color figure can be viewed at wileyonlinelibrary.com]

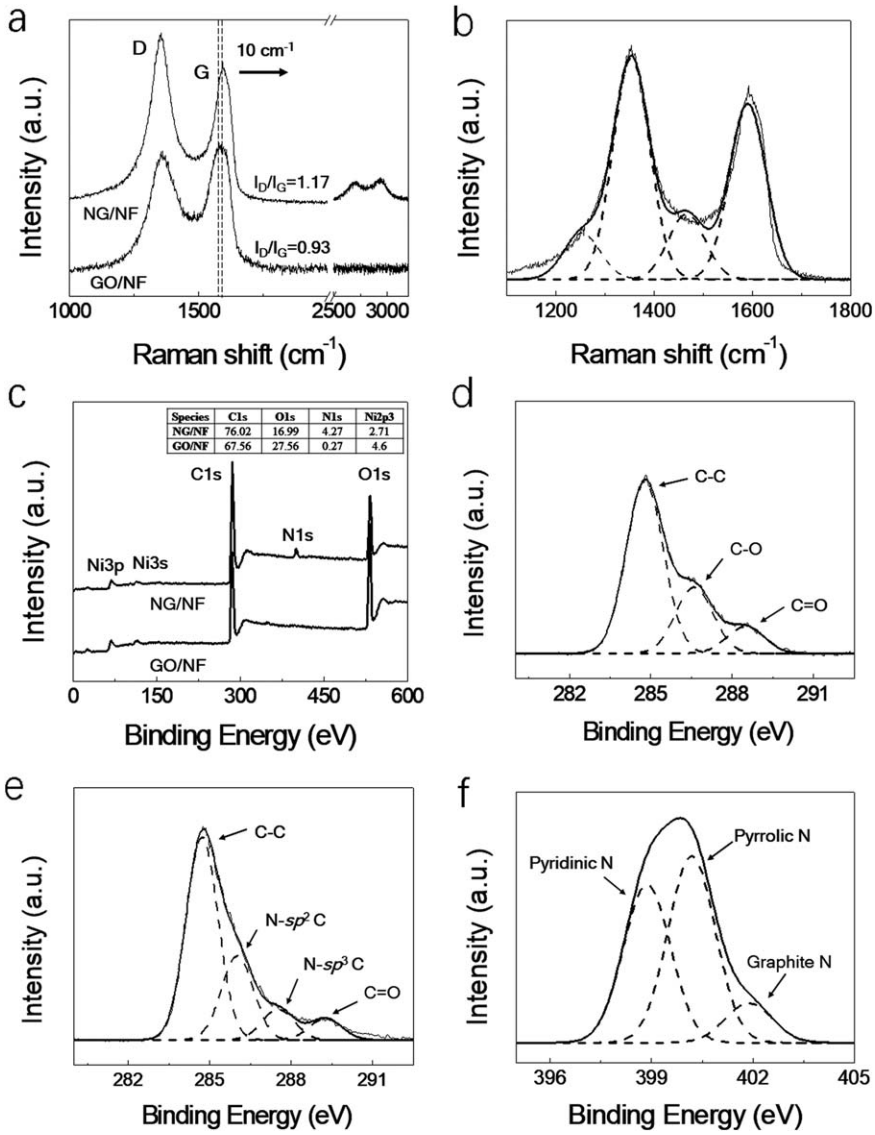

Figure 3. (a) Raman spectra of NG/NF and GO/NF, (b) peak fit for NG/NF, (c) XPS spectra of NG/NF and GO/NF, (d) C1s peak fit of GO/NF, (e) C1s peak fit of NG/NF, (f) N1s peak fit of NG/NF.

NG and 3D NF has exhibited high performance in electrochemical catalysis.[30–32] Nevertheless, to the best of our knowledge, the use of 3D-foam-structured nitrogen-doped graphene-Ni (NG/NF) catalysts for the reduction of nitrobenzene has been rarely reported.

Herein, we report the preparation of a 3D-foam-structured NG/NF, its performance as a catalyst for the reduction of nitrobenzene, and detailed studies of the chemical reaction kinetics. The effects of the reaction temperature, superficial area of the catalyst, and concentrations of the initial reactants were investigated. Furthermore, the obtained kinetics data were fit to the Langmuir-Hinshelwood model. Density functional theory (DFT) calculations were also performed to understand the mechanism of the catalytic reaction.

Experimental Section

Materials

NF with a pore density of 30 ppi was purchased from Shenzhen Hexingchuangda Technology Co. Ltd. Graphene oxide (GO), produced by the modified Hummers method, was obtained from Beijing Chemicals Ltd.[33] Nitrobenzene, sodium borohydride, urea, ethanol, acetone, and hydrochloric acid were purchased from Sigma Aldrich. The reagents were all analytically pure and used without additional purification unless otherwise mentioned. Deionized water was prepared by a Hitech laboratory water purification system, Smart-S30 (Shanghai Hitech Instruments Co. Ltd) and used for all experiments.

Preparation of NG/NF

Briefly, raw NF was treated in sequence with acetone and hydrochloric acid for 1 h each to remove contaminants and subsequently washed with ethanol and deionized water. The pretreated NF sheet (2 cm × 1 cm × 0.15 cm) was then soaked in 20 mL of an aqueous GO dispersion (1 mg/mL) under ultrasonic treatment (Kunshan Ultrasonic Instrument Co. Ltd, KQ2200B, 100 W) for 30 min. After that, the GO-coated nickel foam (GO/NF) was removed and dried in air at room temperature for 5 h. For the preparation of NG/NF, the GO/NF was placed in a 50-mL Teflon-lined stainless autoclave with 25 mL of an aqueous urea solution (50 mg/mL) and treated at 180°C for 12 h. The obtained NG/GF was washed

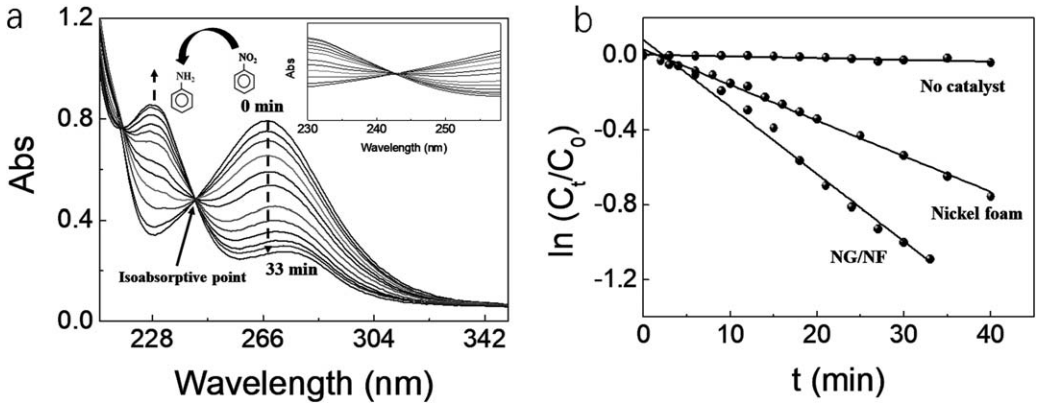

Figure 4. (a) UV/Vis spectra of the reaction solution during catalysis by NG/NF and (b) curves of *ln* (C/C_0) as a function of time. (Reaction conditions: $c_{NB} : c_{NaBH_4} =$ 1:100, room temperature, $m_{catalyst} = 60$ mg, mass loading of NG = 10 wt %).

with water and then dried in air at 60°C for 5 h for further studies of the catalytic performance.

Characterization

Scanning electron microscopy (SEM) imaging and energy-dispersive X-ray (EDX) mapping was performed on a Hitachi S-4700 field emission SEM. Fourier transform infrared (FTIR) spectra were measured on a Thermo Fisher Nicolet 6700 FTIR system. X-ray photoelectron spectroscopy (XPS) measurements were performed on a VG Microtech ESCA 2000 instrument using a monochromic Al X-ray source. Raman spectra were collected on a Renishaw in Via Raman spectrometer using a 514-nm wavelength laser. Catalytic reactions were performed at room temperature and monitored by a Shimadzu UV-2600 UV-Vis scanning spectrophotometer.

Hydrogenation of nitrobenzene

In a typical experiment, 3.5 mL of an aqueous solution containing 1 mmol $NaBH_4$ and 0.01 mmol NB was added to a quartz cuvette (4.5 cm × 1.25 cm × 1.25 cm) along with the NG/NF catalyst (2 cm × 1 cm × 0.15 cm). To investigate the dynamics of the reactions, the NG/NF catalyst was removed from the solution at specified points in the reaction (0–33 min at 3 min intervals), and the absorbance spectrum of the solution was recorded with a UV/vis scanning spectrophotometer. According to the Beer-Lambert law, the absorbance intensity of a chromophore varies linearly with its concentration in a transparent solvent.[34] A set of standard solutions of each chromophore was prepared, and the curve relating the absorbance to the concentration was plotted. The calibration equation shown in Eq. 1 was used to calculate the concentrations of NB and AB at each time point

$$\mathrm{Abs} = \mathrm{A} \times \mathrm{Con} + \mathrm{B} \tag{1}$$

In this equation, A and B are standard values obtained from the calibration plot and represent the slope and intercept, respectively. Con and Abs represent the concentration and absorbance of the solute, respectively. In our experiments, the absorbance intensities of peaks at 267 nm and 232 nm were measured to calibrate the NB and AB concentrations, respectively. Bare NF and GO/NF were also used as catalysts in the nitrobenzene reduction studies as control groups for comparison.

DFT simulation

DFT theoretical calculations were performed by the Dmol^3 code of Materials Studio 8.0 commercial software. The graphene sheet model used in this study included 110 carbon atoms and 28 hydrogen atoms, which eliminated the edge-hydrogen-atom influence on the whole graphene sheet. The doping energy (E_{doping}) was calculated as follows

$$E_{doping} = E_{NG} + E_C - E_{graphene} - E_N \tag{2}$$

where E_{NG} and $E_{graphene}$ are the energies of the optimized structures of nitrogen-doped graphene and intrinsic graphene, respectively. E_C and E_N are the total energies of the carbon and nitrogen atoms, respectively.

The adsorption energy (E_{ads}) of each reactant was calculated to analyze the relative adsorbability to different materials, which is defined by Eq. 3 as follows

$$E_{ads} = E_{total} - E_{graphene} - E_{molecule} \tag{3}$$

where E_{total} is the total energy of the optimized system and $E_{molecule}$ is the energy of the adsorbed molecule.

Results and Discussion

The formation of NG/NF is illustrated in Figure 1. On immersion of a section of NF in an aqueous suspension of GO under ultrasonication, the GO sheets rapidly filled the micropores and then coated the NF network. After the removal of water, strong adhesion of the GO to the surface of the nickel metal occurred through van der Waals interactions.[35,36] During the hydrothermal treatment of GO/NF with urea, the GO sheets were reduced to graphene, and nitrogen was doped into the graphene lattice to form NG/NF composites. As excess GO and urea were used, the surface of NF was estimated to be fully covered with NG owing to the favorable interactions between nickel and GO sheets. The weight ratio of NG to NF was calculated to be 10 wt % based on the weights of the raw NF and the final NG/NF composite. To study the robustness of NG/NF, the release kinetics of NG from NG/NF were investigated by sonication treatment of NG/NF in water. The percentage of NG released from NG/NF was below 1 wt % throughout the sonication treatment (up to 30 min), indicating that the structure of NG/NF was stable (Supporting Information Figure S1).

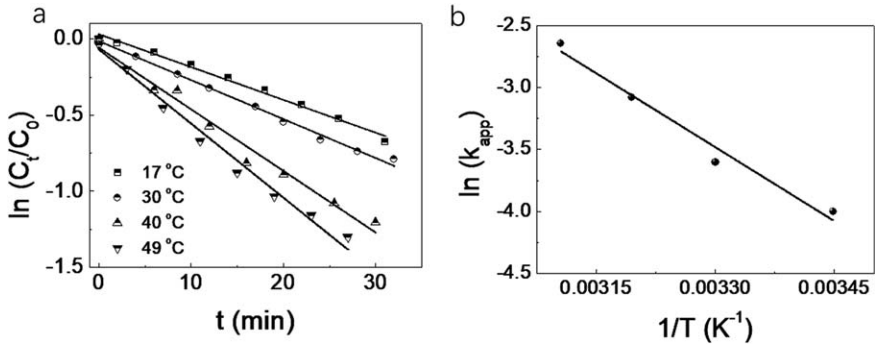

Figure 5. (a) Plot of *ln (C/C$_0$)* vs. time for different reaction temperatures. (b) Plot of *ln (k_{app})* vs. 1/*T*.

Photographs of bare NF and NG/NF under visible light, as well as their microstructures observed by SEM, are presented in Figure 2. Bare NF has a metallic luster (inset in Figure 2a) and a typical 3D cross-linked grid structure with pore sizes ranging between 100 and 300 μm (Figure 2a). NG/NF appears dark black (inset in Figure 2b) because the entire NF scaffold is covered with NG sheets (Figure 2b). There are no obvious differences between the SEM images of NF and NG/NF, indicating that the framework of NF was stable during the NG coating process. In the elemental mapping of C, N, and O in a typical SEM image of NG/NF, the signals of C, N, and O, which came from NG, can be clearly observed in the NF network, indicating that the NF was fully covered with NG (Figures 2c–f). The FTIR spectrum of NG/NF (Supporting Information Figure S2) shows the characteristic peaks of C = N and C-N stretching vibrations at 1384 cm^{-1} and 1165 cm^{-1}, respectively, which also demonstrates the successful deposition of N-doped graphene on the NF.

The presence of NG sheets and their structural composition on NG/NF were further confirmed by Raman spectroscopy and XPS analysis. According to the Raman spectra shown in Figure 3a, the ratio of the D to G bands intensities (I_D/I_G) for NG/NF and GO/NF are 1.17 and 0.93, indicating that the degree of defects in NG/NF was higher than that in GO/NF.[37] The G band of NG/NF exhibits a blueshift of approximately 10 cm^{-1} relative to that of GO/NF, which was attributed to the doping of N atoms.[38] As shown in Figure 3b, the Raman peaks of NG/NF were deconvoluted into four curves with peaks at 1250 cm^{-1}, 1355 cm^{-1} (D band), 1450 cm^{-1} and 1600 cm^{-1} (G band). The D and G bands reflect the defects in graphene, while the bands at 1250 cm^{-1} and 1450 cm^{-1} were attributed to the carbon atoms outside the intrinsic graphene molecules and the change in the graphene structure, respectively. The XPS spectra shown in Figure 3c also demonstrate the successful doping of nitrogen in NG/NF, with an N atomic percentage of 4.3%. The C1s XPS spectrum of GO/NF shown in Figure 3d indicates the presence of three types of carbon bond in GO/NF: graphite sp^2 C (284.71 eV), C-O (286.6 eV), and C = O (289.20 eV). However, four types of carbon bonds, graphite sp^2 C (284.71 eV), N-sp^2 C (286.05 eV), N-sp^3 C (287.55 eV), and C = O (289.20 eV), were observed in the C1s XPS spectrum of NG/NF (Figure 3e), suggesting that nitrogen was doped into the graphene structure. The N1s XPS spectrum of NG/NF shown in Figure 3f indicates the presence of three

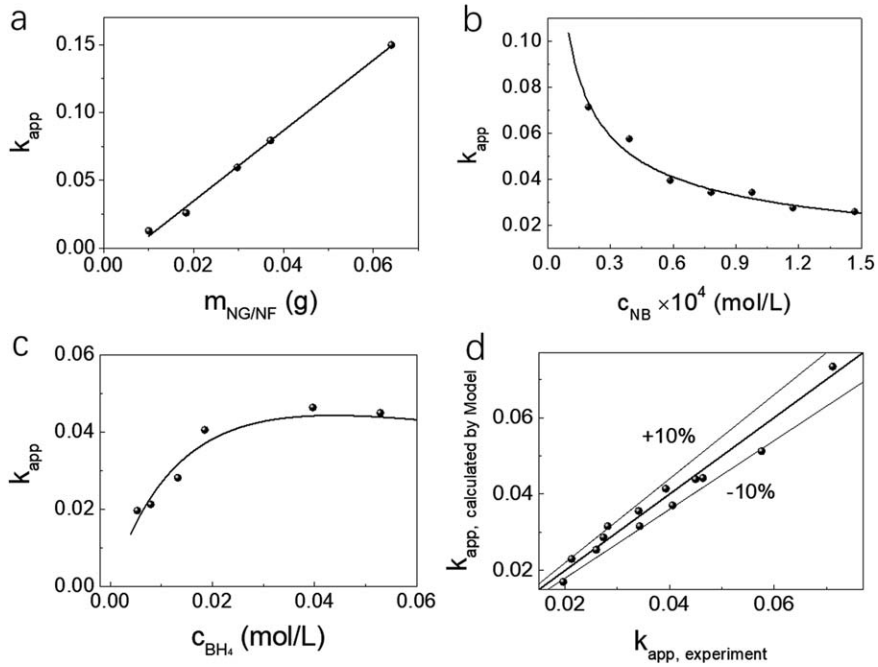

Figure 6. k_{app} as a function of (a) catalyst amount, (b) concentration of NB, and (c) concentration of $NaBH_4$. (d) Comparison of the theoretical (L-H equation) and experimental k_{app} values.

types of C-N bonds, which are pyridinic N (398.85 eV), pyrrolic N (400.2 eV) and graphitic N (401.9 eV), with relative contents of 41.13%, 48.59%, and 10.28%, respectively.

The electron density distribution of graphene is known to become asymmetric after doping nitrogen atoms into the nanocarbon molecules,[39,40] resulting in a higher positive charge density and spin density on the carbon atoms next to the doped N atoms (Supporting Information Figure S3). The highest occupied molecular orbitals (HOMOs) and lowest unoccupied molecular orbitals (LUMOs) of intrinsic graphene, graphitic N, pyridinic N, and pyrrolic N are shown in Supporting Information Figure S4. The main difference between the doped graphene and intrinsic graphene is that the electron distribution in the LUMO became more uniform following the introduction of nitrogen, which results in a better electron accepting ability of the nitrogen-doped graphene. In our experiments, the doping energies (E_{doping}) of graphitic N, pyridinic N and pyrrolic N were calculated as 3.54, 2.929 and 2.316 eV, respectively (Supporting Information Table S1). These theoretically calculated results suggest that pyrrolic N exhibits the lowest doping energy, which means that this type of N-C bond is the most likely to be introduced into the graphene units. These results are consistent with the XPS analysis (Figure 3f).

The performance of NG/NF as a catalyst for the reduction of NB is presented in Figure 4. As shown in the absorbance spectra given in Figure 4a, the intensity of the NB absorbance peak at 267 nm rapidly decreased due to the reaction of NB with $NaBH_4$ in the solution. An absorbance peak at 232 nm, which is the characteristic absorbance peak of AB based on the absorbance spectrum of AB shown in Supporting Information Figure S5, grew as the reaction continued, indicating the formation of AB from the reduction of NB. The presence of an isosbestic point at 243 nm illustrates that no by-products formed during the reaction.[41] The reaction was continuously monitored for over 30 min, and Figure 4b gives the curve of $ln\ (C_t/C_0)$ as a function of the reaction time, where C_0 is the initial concentration of NB and C_t represents the concentration of NB at each time point. The results given in Figure 4b show that the reduction of NB to AB by $NaBH_4$ in the presence of NG/NF as the catalyst followed pseudofirst-order kinetics. However, when no catalyst was used, very little NB was reduced over 2 h, even when excess $NaBH_4$ was added into the NB solution (Supporting Information Figure S6a). When GO/NF was used as the catalyst, a decrease in the absorbance intensity of NB in the solution was observed, but the absorbance peak corresponding to AB did not appear (Supporting Information Figure S6b), suggesting that the decrease in the NB peak was caused by the physical adsorption of NB to the graphene oxide. Therefore, the nitrogen doping of NG/NF was the key factor in the catalytic reduction of NB to AB by $NaBH_4$. The reusability of the catalyst was also investigated, and the activity of NG/NF decreased by no more than 20% after eight cycles (Supporting Information Figure S7).

The catalytic reduction of NB by NG/NF at various reaction temperatures (17, 30, 40, and 49°C) was further investigated, and the corresponding plots of $ln\ (C_t/C_0)$ vs. time (t) are shown in Figure 5a. As the reaction of NB to AB exhibited pseudofirst-order kinetics in our experiments, the apparent kinetic rate constant (k_{app}) for the reaction was calculated from the following Eq. 4. The plot of ln (k_{app}) vs. the inverse of temperature (K^{-1}) is presented in Figure 5b

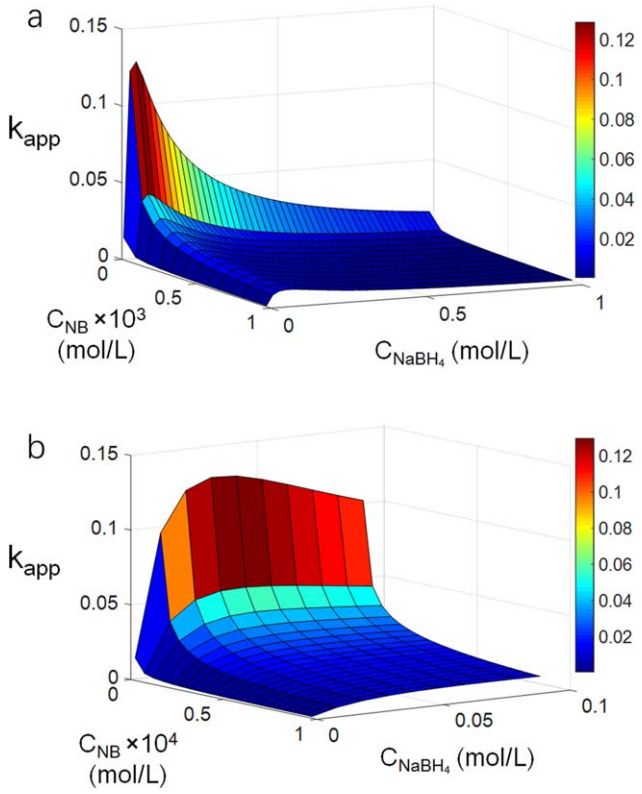

Figure 7. k_{app} values calculated by the L-H equation as a function of C_{NB} and $C_{BH_4^-}$.

(a) 3D plot of k_{app} vs. C_{NB} and $C_{BH_4^-}$ with $C_{BH_4^-}$ from 0.0 to 1.0 mol/L and C_{NB} from 0.0 to 1 × 10^{-3} mol/L and (b) an enlarged plot of (a) showing $C_{BH_4^-}$ from 0.0 to 0.1 mol/L and C_{NB} from 0.0 to 1 × 10^{-4} mol/L. [Color figure can be viewed at wileyonlinelibrary.com]

$$\ln\left(\frac{C_t}{C_0}\right) = k_{app} \cdot t \tag{4}$$

In this equation, C_0 and C_t represent the initial concentration of NB and the concentration of NB at a given time point in the reaction, respectively; k_{app} is the apparent kinetic rate constant; and t is the reaction time.

The reaction system exhibited a strong dependence of k_{app} on the temperature, corresponding to a gradual increase in the solubility as the temperature increased in the range of 17–49°C. These experimental results can be explained by the collision theory. With increasing reaction temperature, the molecular movement becomes more violent, resulting in a greater chance of collision, which then causes an increase in the apparent reaction rate.[42] The apparent activation energy (E_a) was calculated to be 30.50 kJ/mol according to the Arrhenius equation given in Eq. 5

$$\ln k_{app} = \ln A - \frac{E_a}{RT} \tag{5}$$

In this equation, E_a is the apparent activation energy, A is a pre-exponential factor, and R is the general gas constant ($R = 8.314$ J/[K·mol]).

As the catalytic reduction of NB to AB is a type of surface transfer reaction and requires coadsorption of the reactants to the surface of the catalyst, the reaction parameters, such as the superficial area of the catalyst and the initial concentrations of NB (C_{NB}) and $NaBH_4$ ($C_{BH_4^-}$), play important roles in determining the value of k_{app}. In this work, the effects of such

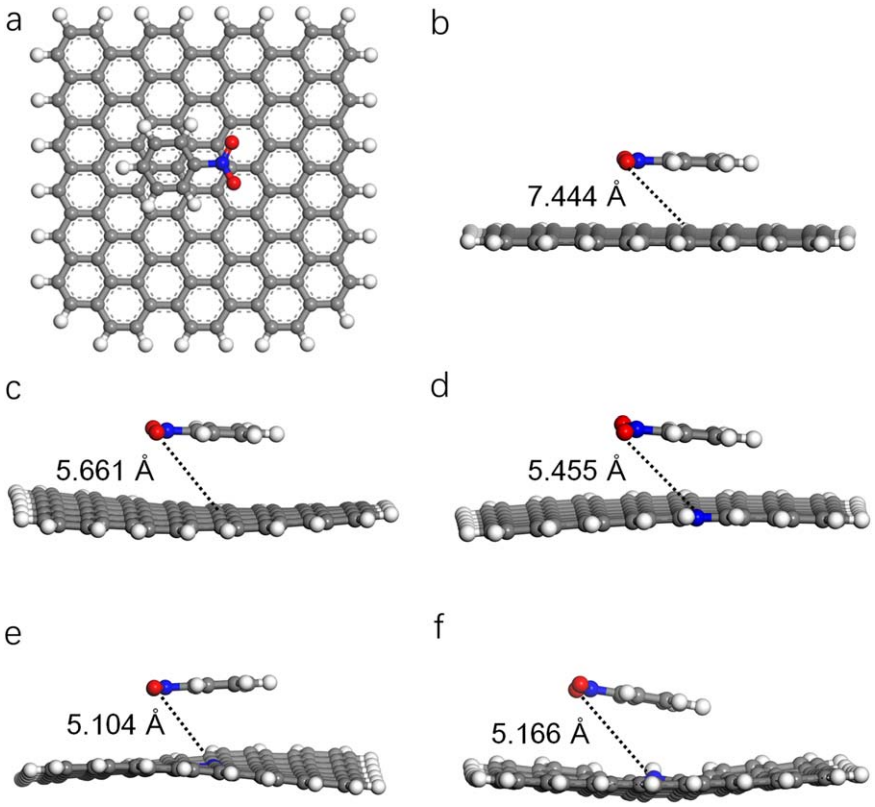

Figure 8. Optimized structures of the NB molecule before adsorption at the center of pristine graphene from the (a) top view and (b) side view. Optimized structures of the NB molecule adsorbed on (c) pristine graphene, (d) pyridinic N, (e) graphitic N and (f) pyrrolic N. The gray, blue, red and white spheres represent C, N, O, and H atoms, respectively.

[Color figure can be viewed at wileyonlinelibrary.com]

reaction parameters were evaluated through single factor experiments at room temperature. For NG/NF, the superficial area was directly proportional to the mass of NG/NF. Figure 6a shows the plot of k_{app} as a function of the mass of the NG/NF catalyst, in which the value of k_{app} increases with increasing mass of NG/NF. In that experiment, the values of C_{NB} and $C_{BH_4^-}$ were 9.788×10^{-5} mol/L and 0.0132 mol/L, respectively. Figures 6b, c show the dependence of k_{app} on C_{NB} and $C_{BH_4^-}$, respectively. Under the conditions of constant $C_{BH_4^-}$ (0.0132 mol/L) and $m_{NG/NF}$ (20 mg), k_{app} monotonically decreased with increasing C_{NB}. In contrast, under constant C_{NB} (9.788×10^{-5} mol/L) and $m_{NG/NF}$ (20 mg), k_{app} first increased and then decreased with increasing $C_{BH_4^-}$. These results suggest that during the reaction, the borohydride ions first adsorbed to the surface of NG and then transferred hydrogen to form a surface-bound hydrogen species, which was followed by the adsorption of NB molecules to the catalyst. This mechanism agrees with previous reports on NB reduction by $NaBH_4$ in the presence of metal catalysts.[43]

The above experimental results were then fitted by the Langmuir-Hinshelwood (L-H) model[44]

$$\frac{dC_{NB}}{dt} = -k \cdot S \cdot \theta_{NB} \cdot \theta_{BH_4^-} \tag{6}$$

In this equation, k is the intrinsic rate constant, and θ_{NB} and $\theta_{BH_4^-}$ are the surface coverages of NB and BH_4^- on NG/NF, respectively, which can be modeled by Langmuir isotherms as follows

$$\theta_{NB} = \frac{(K_{NB} \cdot C_{NB})^n}{1 + (K_{NB} \cdot C_{NB})^n + \left(K_{BH_4^-} \cdot C_{BH_4^-}\right)^m}$$
$$\theta_{BH_4^-} = \frac{\left(K_{BH_4^-} \cdot C_{BH_4^-}\right)^m}{1 + (K_{NB} \cdot C_{NB})^n + \left(K_{BH_4^-} \cdot C_{BH_4^-}\right)^m} \tag{7}$$

where K_{NB} and $K_{BH_4^-}$ are the adsorption constants of NB and BH_4^-, respectively, and C_{NB} and $C_{BH_4^-}$ are their corresponding concentrations in solution.

Therefore, k_{app} can be derived from the substitution of Eq. 7 into Eq. 6 and finally expressed as follows

$$k_{app} = \frac{k \cdot S \cdot K_{NB}^n \cdot C_{NB}^{n-1} \cdot K_{BH_4^-}^m \cdot C_{BH_4^-}^m}{\left(1 + (K_{NB} \cdot C_{NB})^n + \left(K_{BH_4^-} \cdot C_{BH_4^-}\right)^m\right)^2} \tag{8}$$

The parameters in the model were calculated, and the results are listed in Supporting Information Table S2. The plot of the k_{app} values predicted by the L-H model vs. the experimental values of k_{app} is presented in Figure 6d. The deviation between the two groups was less than 10%, indicating that the experimental kinetics data fit well to the L-H model.

Furthermore, the 3D plot of k_{app} vs. C_{NB} and $C_{BH_4^-}$ obtained from the calculated L-H equation (Eq. 9) is shown in Figure 7a. The calculated L-H equation is expressed as follows

$$k_{app} = \frac{0.2 \cdot C_{NB}^{-0.5} \cdot C_{BH_4^-}}{\left(1 + 4.58 \cdot C_{NB}^{0.5} + 23.94 \cdot C_{BH_4^-}\right)^2} \tag{9}$$

which then transforms to

$$k_{app} = \frac{0.2}{C_{NB}^{0.5} \times \left(1 + 4.58 \cdot C_{NB}^{0.5}\right)^2 \cdot \frac{1}{C_{BH_4^-}} + 47.88 \times \left(1 + 4.58 \cdot C_{NB}^{0.5}\right) + 573.1236 \cdot C_{BH_4^-}} \quad (10)$$

According to Eq. 10, k_{app} and C_{NB} are negatively correlated, that is, when the concentration of NB increases, the value of k_{app} gradually decreases. This trend agrees well with the experimental results shown in Figure 6b. The relationship between k_{app} and $C_{BH_4^-}$ can be described by a basic quadratic equation. Therefore, k_{app} first increased to a maximum value and then decreased with increasing $C_{BH_4^-}$. From the enlarged plot shown in Figure 7b, the optimized concentration of $NaBH_4$ for the reduction of low concentrations of NB in the above catalytic reaction system was identified as 0.025 mol/L.

DFT calculations were then performed to further understand the catalytic reduction of NB to AB with NG/NF as the catalyst. The graphene sheet has a perfectly planar structure before adsorbing a NB molecule (Figures 8a, b). However, both graphene and NG exhibit varying degrees of distortion on adsorption of the NB molecule via close interaction with a carbon atom near the edge (intrinsic graphene) or next to a doped nitrogen atom (NG) (Figures 8c–f). The distance between the C-O bond of the NB molecule and the NG sheet was approximately 5 Å. The adsorption energy of NB on intrinsic graphene, graphitic N, pyridinic N and pyrrolic N was calculated as 0.182, 0.195, 0.189, and 0.265 eV, respectively (Supporting Information Table S1). The adsorption energies of $NaBH_4$ and NB on the graphitic N-doped graphene was obtained, and the ratio of their energies ($E_{ads-NB} : E_{ads-NaBH_4} = 1.145$) matched well to the ratio of K_{NB} and $K_{NaBH_4^-}$ ($K_{NB} : K_{NaBH_4} = 1.14$) obtained by fitting the experimental data to the L-H model. These results also demonstrate the prior adsorption of $NaBH_4$ in the reaction process.[11,41]

Conclusions

A porous 3D-foam-structured NG/NF catalyst was prepared by a hydrothermal method, and the catalyst exhibited high performance in the reduction of nitrobenzene. The separation of the 3D-foam-structured catalyst from the products was more convenient than that of traditional powdered catalysts, and therefore, this catalyst holds more promise for industrial applications. Kinetics studies of the catalytic reduction process were performed under various conditions, including different reaction temperatures, catalyst dosages and initial concentrations of reactants. The NG/NF catalyst showed a significantly higher reaction rate than bare NF and a graphene oxide-coated NF. The obtained kinetics data fit well to the Langmuir-Hinshelwood model, with an error ratio below 10%. Density functional theory (DFT) calculations indicated that the adsorption of sodium borohydride ($NaBH_4$) on NG/NF was stronger than that of NB, which strongly agreed with the kinetic parameters determined from the Langmuir-Hinshelwood model.

Acknowledgments

We are grateful for financial support from the National Natural Science Foundation of China (21620102007 and 21622601), the Fundamental Research Funds for the Central Universities of China (BUCTRC201601), and the "111" project of China (B14004).

Literature Cited

1. Zhu J, Shen Y, Gu F, Tao J, Zhang J. Preparation and photovoltaic properties of near-infrared absorbing manganese(II) phthalocyanine polymer films. *Mater Lett*. 2007;61(6):1296–1298.
2. Jiang Y, Li X, Qin Z, Ji H. Preparation of Ni/bentonite catalyst and its applications in the catalytic hydrogenation of nitrobenzene to aniline. *Chin J Chem Eng*. 2016;24(9):1195–1200.
3. Palmisano G, Loddo V, Augugliaro V, Palmisano L, Yurdakal S. Photocatalytic oxidation of nitrobenzene and phenylamine: pathways and kinetics. *AIChE J*. 2007;53(4):961–968.
4. Rodriguez M, Timokhin V, Michl F, Contreras S, Gimenez J, Esplugas S. The influence of different irradiation sources on the treatment of nitrobenzene. *Catal Today*. 2002;76(2–4):291–300.
5. Mu Y, Yu H-Q, Zheng J-C, Zhang S-J, Sheng G-P. Reductive degradation of nitrobenzene in aqueous solution by Zero-valent iron. *Chemosphere*. 2004;54(7):789–794.
6. Li C, Zhang X, Hao X, Wang M, Ding C, Wang Z, Wang Y, Guan G, Abudula A. Efficient recovery of high-purity aniline from aqueous solutions using pervaporation-fractional condensation system. *AIChE J*. 2015;61(12):4445–4455.
7. Yang XJ, Tian PF, Zhang XM, Yu X, Wu T, Xu J, Han YF, Cheng R. The generation of hydroxyl radicals by hydrogen peroxide decomposition on FeOCl/SBA-15 catalysts for phenol degradation. *AIChE J*. 2015;61(1):166–176.
8. Gelder EA, Jackson SD, Lok CM. A study of nitrobenzene hydrogenation over Palladium/Carbon catalysts. *Catal Lett*. 2002;84(3/4):205–208.
9. Zhang S, Li L, Liu Y, Zhang Q. TiO_2-SA-Arg nanoparticles stabilized Pickering emulsion for photocatalytic degradation of nitrobenzene in a rotating annular reactor. *Chin J Chem Eng*. 2017;25(2):223–231.
10. Lang Y, Wang Q, Xing J, Zhang B, Liu H. Preparation of magnetic γ-Al_2O_3 supported palladium catalyst for hydrogenation of nitrobenzene. *AIChE J*. 2008;54(9):2303–2309.
11. Ansar SM, Kitchens CL. Impact of gold nanoparticle stabilizing ligands on the colloidal catalytic reduction of 4-nitrophenol. *ACS Catal*. 2016;6(8):5553–5560.
12. Chen P, Yang F, Kostka A, Xia W. Interaction of cobalt nanoparticles with oxygen- and nitrogen-functionalized carbon nanotubes and impact on nitrobenzene hydrogenation catalysis. *ACS Catal*. 2014;4(5):1478–1486.
13. Zhao Z, Dai Y, Ge G, Wang G. Efficient tuning of microstructure and surface chemistry of nanocarbon catalysts for ethylbenzene direct dehydrogenation. *AIChE J*. 2015;61(8):2543–2561.
14. Su DS, Perathoner S, Centi G. Nanocarbons for the development of advanced catalysts. *Chem Rev*. 2013;113(8):5782–5816.
15. Tan C, Su X, Zhou C, Wang B, Zhan Q, He S. Acid-assisted hydrothermal synthesis of red fluorescent carbon dots for sensitive detection of Fe(III). *RSC Adv*. 2017;7(65):40952–40956.
16. Wang D, Wang Z, Zhan Q, Pu Y, Wang J, Foster N, Dai L. Facile and scalable preparation of fluorescent carbon dots for multifunctional applications. *Engineering*. 2017;3(3):402–408.
17. Kong X, Liu Q, Zhang C, Peng Z, Chen Q. Elemental two-dimensional nanosheets beyond graphene. *Chem Soc Rev*. 2017;46(8):2127–2157.
18. Esfandiyari T, Nasirizadeh N, Dehghani M, Ehrampoosh MH. Graphene oxide based carbon composite as adsorbent for Hg removal: preparation, characterization, kinetics and isotherm studies. *Chin J Chem Eng*. 2017;25(9):1170–1175.
19. Zhang Y, Dong N, Tao H, Yan C, Huang J, Liu T, Robertson A, Texter J, Wang J, Sun Z. Exfoliation of stable 2D black phosphorus for device fabrication. *Chem Mater*. 2017;29(15):6445–6456.
20. Tao H, Gao Y, Talreja N, Guo F, Texter J, Yan C, Sun Z. Two-dimensional nanosheets for electrocatalysis in energy generation and conversion. *J Mater Chem A*. 2017;5(16):7257–7284.
21. Xiang Z, Dai Q, Chen JF, Dai L. Edge functionalization of graphene and two-dimensional covalent organic polymers for energy conversion and storage. *Adv Mater*. 2016;28(29):6253–6261.

22. Wang D, Chen JF, Dai L. Recent advances in graphene quantum dots for fluorescence bioimaging from cells through tissues to animals. *Part Part Syst Charact*. 2015;32(5):515–523.
23. Wang H, Maiyalagan T, Wang X. Review on recent progress in nitrogen-doped graphene: synthesis, characterization, and its potential applications. *ACS Catal*. 2012;2(5):781–794.
24. Su C, Loh KP. Carbocatalysts: graphene oxide and its derivatives. *Acc Chem Res*. 2013;46(10):2275–2285.
25. Tschentscher R, Nijhuis TA, Schaaf J, Kuster BM, Schouten JC. Gas-liquid mass transfer in rotating solid foam reactors. *Chem Eng Sci*. 2010;65(1):472–479.
26. Chu GW, Song YJ, Zhang WJ, Luo Y, Zou HK, Xiang Y, Chen JF. Micromixing efficiency enhancement in a rotating packed bed reactor with surface-modified nickel foam packing. *Ind Eng Chem Res*. 2015;54(5):1697–1702.
27. Marín P, Hevia MG, Ordonez S, Díez F. Combustion of methane lean mixtures in reverse flow reactors: comparison between packed and structured catalyst beds. *Catal Today*. 2005;105(3–4):701–708.
28. Chen Y, Zhang X, Yu P, Ma Y. Electrophoretic deposition of graphene nanosheets on nickel foams for electrochemical capacitors. *J Power Sources*. 2010;195(9):3031–3035.
29. Wang H, Wang G, Ling Y, Qian F, Song Y, Lu X, Chen S, Tong Y, Li Y. High power density microbial fuel cell with flexible 3D graphene-nickel foam as anode. *Nanoscale*. 2013;5(21):10283–10290.
30. Huang H, Lei C, Luo G, Cheng Z, Li G, Tang S, Du Y. Facile synthesis of nitrogen-doped graphene on Ni foam for high-performance supercapacitors. *J Mater Sci*. 2016;51(13):6348–6356.
31. Chen J, Sheng K, Luo P, Li C, Shi G. Graphene hydrogels deposited in nickel foams for high-rate electrochemical capacitors. *Adv Mater*. 2012;24(33):4569–4573.
32. Chang YH, Lin CT, Chen TY, Hsu CL, Lee YH, Zhang W, Wei KH, Li LJ. Highly efficient electrocatalytic hydrogen production by MoS(x) grown on graphene-protected 3D Ni foams. *Adv Mater*. 2013;25(5):756–760.
33. Qian J, Wang D, Cai FH, Xi W, Peng L, Zhu ZF, He H, Hu ML, He S. Observation of multiphoton-induced fluorescence from graphene oxide nanoparticles and applications in in vivo functional bioimaging. *Angew Chem Int Ed*. 2012;51(42):10570–10575.
34. Wang D, Qian J, He S, Park JS, Lee KS, Han S, Mu Y. Aggregation-enhanced fluorescence in PEGylated phospholipid nanomicelles for *in vivo* imaging. *Biomaterials*. 2011;32(25):5880–5888.
35. Huang H, Xu L, Tang Y, Tang S, Du Y. Facile synthesis of nickel network supported three-dimensional graphene gel as a lightweight and binder-free electrode for high rate performance supercapacitor application. *Nanoscale*. 2014;6(4):2426–2433.
36. Bekyarova E, Sarkar S, Wang F, Itkis ME, Kalinina I, Tian X, Haddon RC. Effect of covalent chemistry on the electronic structure and properties of carbon nanotubes and graphene. *Acc Chem Res*. 2013;46(1):65–76.
37. Ruan G, Sun Z, Peng Z, Tour JM. Growth of graphene from food, insects, and waste. *ACS Nano*. 2011;5(9):7601–7607.
38. Wu ZS, Winter A, Chen L, Sun Y, Turchanin A, Feng X, Müllen K. Three-dimensional nitrogen and boron co-doped graphene for high-performance all-solid-state supercapacitors. *Adv Mater*. 2012;24(37):5130–5135.
39. Gong K, Du F, Xia Z, Durstock M, Dai L. Nitrogen-doped carbon nanotube arrays with high electrocatalytic activity for oxygen reduction. *Science*. 2009;323(5915):760–764.
40. Li X, Pan X, Yu L, Ren P, Wu X, Sun L, Jiao F, Bao X. Silicon carbide-derived carbon nanocomposite as a substitute for mercury in the catalytic hydrochlorination of acetylene. *Nat Commun*. 2014;5:3688–3694.
41. Kästner C, Thünemann AF. Catalytic reduction of 4-nitrophenol using silver nanoparticles with adjustable activity. *Langmuir*. 2016;32(29):7383–7391.
42. Nemanashi M, Meijboom R. Synthesis and characterization of Cu, Ag and Au dendrimer-encapsulated nanoparticles and their application in the reduction of 4-nitrophenol to 4-aminophenol. *J Colloid Interface Sci*. 2013;389(1):260–267.
43. Wunder S, Lu Y, Albrecht M, Ballauff M. Catalytic activity of faceted gold nanoparticles studied by a model reaction: evidence for substrate-induced surface restructuring. *ACS Catal*. 2011;1(8):908–916.
44. Wan Y, Zhou Z, Cheng Z. Hydrogen production from steam reforming of methanol over $CuO/ZnO/Al_2O_3$ catalysts: Catalytic performance and kinetic modeling. *Chin J Chem Eng*. 2016;24(9):1186–1194.

Manuscript received Apr. 23, 2017, and revision received Oct. 15, 2017.